



CHALMERS
UNIVERSITY OF TECHNOLOGY

Raster Image Correlation Spectroscopy Performance Evaluation

Downloaded from: <https://research.chalmers.se>, 2025-04-24 13:47 UTC

Citation for the original published paper (version of record):

Longfils, M., Smisdorn, N., Ameloot, M. et al (2019). Raster Image Correlation Spectroscopy Performance Evaluation. *Biophysical Journal*, 117(10): 1900-1914.
<http://dx.doi.org/10.1016/j.bpj.2019.09.045>

N.B. When citing this work, cite the original published paper.

Raster Image Correlation Spectroscopy Performance Evaluation

Marco Longfils,^{1,*} Nick Smisdom,^{2,3} Marcel Ameloot,³ Mats Rudemo,¹ Veerle Lemmens,^{3,4,5} Guillermo Solís Fernández,⁶ Magnus Röding,⁶ Niklas Lorén,^{6,7} Jelle Hendrix,^{3,4,*} and Aila Särkkä¹

¹Department of Mathematical Sciences, Chalmers University of Technology and University of Gothenburg, Gothenburg, Sweden; ²Stadius Centre for Dynamical Systems, Signal Processing and Data Analytics, KU Leuven, Leuven, Belgium; ³Advanced Optical Microscopy Centre, Biomedical Research Institute and ⁴Dynamic Bioimaging Lab, Hasselt University, Diepenbeek, Belgium; ⁵Molecular Imaging and Photonics, Chemistry Department, KU Leuven, Heverlee, Belgium; ⁶RISE Bioscience and Materials, Gothenburg, Sweden; and ⁷Department of Physics, Chalmers University of Technology, Gothenburg, Sweden

ABSTRACT Raster image correlation spectroscopy (RICS) is a fluorescence image analysis method for extracting the mobility, concentration, and stoichiometry of diffusing fluorescent molecules from confocal image stacks. The method works by calculating a spatial correlation function for each image and analyzing the average of those by model fitting. Rules of thumb exist for RICS image acquisition, yet a rigorous theoretical approach to predict the accuracy and precision of the recovered parameters has been lacking. We outline explicit expressions to reveal the dependence of RICS results on experimental parameters. In terms of imaging settings, we observed that a twofold decrease of the pixel size, e.g., from 100 to 50 nm, decreases the error on the translational diffusion constant (D) between three- and fivefold. For $D = 1 \mu\text{m}^2 \text{s}^{-1}$, a typical value for intracellular measurements, ~ 25 -fold lower mean-squared relative error was obtained when the optimal scan speed was used, although more drastic improvements were observed for other values of D . We proposed a slightly modified RICS calculation that allows correcting for the significant bias of the autocorrelation function at small ($\ll 50 \times 50$ pixels) sizes of the region of interest. In terms of sample properties, at molecular brightness $E = 100$ kHz and higher, RICS data quality was sufficient using as little as 20 images, whereas the optimal number of frames for lower E scaled pro rata. RICS data quality was constant over the nM– μ M concentration range. We developed a bootstrap-based confidence interval of D that outperformed the classical least-squares approach in terms of coverage probability of the true value of D . We validated the theory via in vitro experiments of enhanced green fluorescent protein at different buffer viscosities. Finally, we outline robust practical guidelines and provide free software to simulate the parameter effects on recovery of the diffusion coefficient.

SIGNIFICANCE Raster image correlation spectroscopy is a fluorescence microscopy method increasingly used in the life and material sciences to estimate the mobility, concentration, and binding ratio of diffusing molecules from confocal laser scanning image series. Here, a theoretical framework is laid out to predict the optimal values of microscope image acquisition parameters (e.g., scan speed, pixel size, image size, probe brightness) to quantify molecular properties with the highest accuracy and precision and benchmarked against both simulated and experimental data. With this new information, quantitatively justified rules of thumb for raster image correlation spectroscopy experimenters are provided. For efficient and widespread application, an easy-to-use and open source software is shared to make such predictions per se.

INTRODUCTION

Since the introduction of image correlation spectroscopy (ICS) (1), the family of image correlation spectroscopy methods has grown richer with the appearance of novel var-

iants of previous techniques. All ICS methods analyze the fluctuations of the fluorescence signal to quantify relevant parameters of the processes that cause the fluctuations. These methods can be classified based on whether fluctuations are considered in time and/or in space. Temporal ICS (TICS) enables the examination of diffusion-related processes (2,3) by studying the correlation of the fluorescence fluctuations over time for each pixel of an image time series. Raster ICS (RICS) was first introduced in (4)

Submitted April 17, 2019, and accepted for publication September 30, 2019.

*Correspondence: longfils@chalmers.se or jelle.hendrix@uhasselt.be

Editor: Jochen Mueller.

<https://doi.org/10.1016/j.bpj.2019.09.045>

© 2019 Biophysical Society.

as a method to study molecular transport in solution and in cells. RICS registers both the temporal and the spatial intensity fluctuations by scanning a laser beam over a sample and exploits the fast pixel-to-pixel and line-to-line sampling to analyze the fluctuations on a faster timescale than TICS. The fluorescence intensity fluctuations are caused by the dynamics of the particles, including, but not limited to, diffusion, flow, and binding. In addition, they are influenced by possible sources of noise such as dark current and shot noise. In RICS, the fluorescence fluctuations autocorrelation function is mainly used to determine macroscopic phenomenological parameters such as the diffusion coefficient and the concentration of the molecule of interest. These parameter estimates can be obtained by fitting the model autocorrelation function to the empirical autocorrelation computed from a series of images. It is well-known that RICS is sensitive to the choice of experimental parameters. For example, the scan speed should be adjusted to the movement of the probe considered. Guidelines on how to set crucial instrumental and sample parameters for acquiring RICS data have been published (5,6). However, the relationship between the various instrumental and molecular parameters and the accuracy and precision in the determination of the diffusion coefficient has not been comprehensively investigated.

This is in contrast to the numerous studies devoted to the statistical accuracy of the nonimaging variant fluorescence correlation spectroscopy (FCS) (7). In the seminal work by Koppel (8), a theoretical analysis of the statistical accuracy of FCS was presented under the assumptions of uniform illumination profile, relatively high concentration of the molecule of interest, and an exponential correlation function. Subsequently, (9) extended Koppel's work to a two-dimensional (2D) Gaussian illumination profile and low concentrations. Later on, (10) showed that Koppel's formula was capable of predicting the standard deviation (SD) of the FCS correlation function for sufficiently simple systems but failed for complex systems such as mixtures of particles. Moreover, (10) highlighted that proper weighting of the correlation function is fundamental in parameter estimation. Thus, they experimentally computed the SD of the correlation function in FCS from the intensity traces in different ways. Later on, (11) derived analytical equations for the bias and variance of the FCS correlation function and validated and used them as a way to optimize the experimental conditions. In all the FCS studies mentioned above, the focus was on the derivation of the signal/noise ratio of an FCS experiment, defined as the ratio of the correlation function/its SD. The signal/noise ratio cannot be directly translated to the statistical determination of the parameter estimates because the correlation function is nonlinear in the parameters of interest. To this end, (12) adopted a maximum likelihood method to estimate the probability of choosing a particular value of the diffusion coefficient against the

correct one. This method was used as a measure of accuracy of FCS as a function of concentration, brightness, and measurement time.

One would expect many of the considerations for FCS to also hold for RICS. However, RICS is characterized by scanning parameters such as pixel dwell time and line time, which are not applicable to FCS. The main advantage of RICS over FCS is the spatial correlation introduced by the scanning beam, which can be used to generate diffusion and concentration maps over the sample.

In this work, we introduce RICS performance evaluation (RICSPE), a method that allows researchers to evaluate the accuracy of RICS given a set of experimental settings and to choose the optimal imaging conditions for an experiment. In [Theory](#), we first briefly recall the fundamentals of RICS and provide analytical formulae for the bias (accuracy) and variance (precision) of the empirical correlation function, which play a major role in RICSPE. Next, we introduce a measure for assessing the accuracy and precision of the diffusion coefficient estimate, the mean-squared relative error, to evaluate the performance of RICS. In the [Results](#), we compare the outcomes obtained by the RICSPE method to the results obtained by molecular Monte Carlo simulations and experiments. Next, we study the effect of changing the different experimental parameters on the diffusion coefficient estimate. We reveal the dependence of RICS results on the probe concentration, brightness, scan speed, pixel size, size of the region of interest (ROI) expressed in pixels, number of frames in the RICS experiment, point spread function (PSF) waist, and measurement time. We confirm our findings with in vitro experiments of enhanced green fluorescent protein at different buffer viscosities. Finally, practical guidelines for the RICS user are summarized in the [Conclusions](#); see [Tables 2](#) and [3](#).

MATERIALS AND METHODS

Theory

Below, we present the theoretical framework needed to evaluate the effect of the imaging conditions on the determination of the diffusion coefficient. First, we outline the background theory of RICS. Second, we introduce analytical formulae for the deviations, both random and systematic, of the empirical correlation function computed from a stack of images from the ideal correlation function, obtained from an experiment with unlimited measurement time. These deviations, discussed in [Bias and Variance of the Empirical Correlation Function](#) and thoroughly determined in the [Supporting Materials and Methods](#), quantify how well the empirical correlation function approximates the ideal one. Third, we propose a simple measure, namely the mean-squared relative error, to assess how well the diffusion coefficient is determined by a set of experimental settings and to compare different imaging conditions. Lastly, we introduce a, to our knowledge, new method to generate realizations of the empirical correlation function in [RICSPE](#). For the convenience of the reader, a list of the most important symbols is given in the [Supporting Materials and Methods](#). A graphical user interface (GUI) is made available in a repository; see the rest of the [Materials](#)

and Methods for more details. The GUI provides a user-friendly environment to perform the RICSPE analysis, and no understanding of the mathematical details or familiarity with the underlying programming language is required.

Principles of RICS

In this section, we briefly recall the RICS theory. More details can be found in (4,13,14). Consider fluorescently labeled, noninteracting particles undergoing diffusion and excited by a laser with an intensity profile approximated by a three-dimensional (3D) Gaussian function

$$I(\vec{r}) = I(x, y, z) = I_0 e^{-\frac{2(x^2+y^2)}{w^2}} e^{-\frac{2z^2}{\alpha^2 w^2}}, \quad (1)$$

$$G(\xi, \psi) = \frac{1}{(X - \xi)(Y - \psi)} \frac{\sum_{i=1}^{X-\xi} \sum_{j=1}^{Y-\psi} \delta F(i, j) \delta F(i + \xi, j + \psi)}{\left(\frac{1}{XY} \sum_{i=1}^X \sum_{j=1}^Y F(i, j) \right)^2}, \quad (4)$$

where I_0 is the central intensity of the laser beam, w is the radius at which the intensity in the focal plane has fallen by a factor e^{-2} , and α is the ratio between the radius at which the intensity along the optical axis has fallen by a factor e^{-2}/w . Because of the dynamics of the particles, the fluorescence intensity $F(x, y)$ of the pixel (x, y) will fluctuate. The fluctuations $\delta F(x, y) = F(x, y) - \langle F \rangle$, where $\langle \cdot \rangle$ indicates spatial average, are analyzed by means of the autocorrelation function (ACF)

$$G_{RICS}(\xi, \psi) = \frac{\langle \delta F(x, y) \delta F(x + \xi, y + \psi) \rangle}{\langle F \rangle^2}, \quad (2)$$

where ξ and ψ are the x and y axis spatial increments in number of pixels, respectively. For a simple model assuming isotropic 3D diffusion of noninteracting particles, the expected correlation function at spatial lag (ξ, ψ) is given by (4)

$$g_D(\xi, \psi) = \frac{1}{N} \exp \left\{ \left[- \frac{(S\xi)^2 + (S\psi)^2}{w^2 + 4D(|\tau_p \xi + \tau_l \psi|)} \right] \right\} \times \left(1 + \frac{4D(|\tau_p \xi + \tau_l \psi|)}{w^2} \right)^{-1} \times \left(1 + \frac{4D(|\tau_p \xi + \tau_l \psi|)}{\alpha^2 w^2} \right)^{-\frac{1}{2}}. \quad (3)$$

Here, N is the average number of particles in the observation volume, D is the diffusion coefficient, S is the pixel size, τ_p the pixel dwell time, and τ_l the line time. The function g_D is referred to as the infinite time ACF because it represents the limit approached by the ACF obtained from an experiment as the measurement time goes to infinity and for a large enough image size yielding very long spatial lags. For simplicity, we omit the factor that accounts for the geometry of the observation volume. This factor depends on the model used to approximate the PSF of the microscope, and widely used models include 3D Gaussian and 2D

Gaussian-Lorentzian functions. We refer to (15) for more details on this subject.

Bias and variance of the empirical correlation function

Because the empirical ACF is an estimator of the infinite time limit ACF, it is crucial to study its statistical properties because these will determine how well the parameters can be estimated. In particular, we investigate the accuracy, i.e., systematic deviation (bias) of the estimator from its expected value, and precision, describing the spread (variance) of a set of measurements of the empirical ACF, that are used in the method described in the next section to evaluate the uncertainties of the estimated diffusion coefficient.

The estimator of the ACF, based on one image with X pixels along a line and Y lines, is (see (1))

which is typically calculated from the inverse Fourier transform of the power spectrum of the image. To derive approximations of the bias and variance of $G(\xi, \psi)$, we Taylor-expand the denominator of $G(\xi, \psi)$ (see Eq. S19 for details) and express the moments of $\delta F(i, j)$ in terms of the experimental parameters (see Eqs. S26–S28). We describe the effect of the dependence bias, i.e., the deviation of the empirical ACF from the infinite time limit ACF due to the statistical dependence of the numerator and denominator in Eq. 4, and the estimation bias, introduced when the average intensity $\langle F \rangle$ is substituted by the estimated average intensity $(1/XY) \sum_{i=1}^X \sum_{j=1}^Y F(i, j)$ (see (16,17)). In particular, see Eq. S21; the dependence bias depends on the third moments of the intensity fluctuations $\delta F(i, j)$. Ignoring the higher-order terms, it can be written as

$$\begin{aligned} \text{Bias}(\xi, \psi) &= \langle G(\xi, \psi) \rangle - g_D(\xi, \psi) = \\ &= - \frac{2}{XY(X - \xi)(Y - \psi)\langle F \rangle^3} \\ &\quad \sum_{i=1}^{X-\xi} \sum_{j=1}^{Y-\psi} \sum_{k=1}^X \sum_{l=1}^Y \langle \delta F(i, j) \delta F(i + \xi, j + \psi) \delta F(k, l) \rangle. \end{aligned} \quad (5)$$

The estimation bias of the normalized ACF, reported in (5,18), cannot be treated analytically. Hence, we rely on simulations and analytical formulae for the unnormalized ACF (see Eq. S15 for details) to study in which experimental conditions the estimation bias is considerable. The estimation bias, in general, can be alleviated by sufficient sampling, which in RICS corresponds to a sufficiently large ROI. We discuss in Effect of the Size of the ROI when the estimation bias is relevant and propose a simple way to correct for it, which we call modified RICS. In modified RICS, in the calculations of the ACF, the average intensity is computed as the average value of all the pixels in the ROI in all images instead of only averaging the pixels in the ROI of a particular image as in standard RICS. The mathematical details are presented in the section ‘‘Bias and Variance’’ in the Supporting Materials and Methods.

Similarly, one can express the variance of $G(\xi, \psi)$ as a function of moments of the fluorescence fluctuations, namely (ignoring the higher-order terms)

$$\begin{aligned} \text{Var}(G(\xi, \psi)) &= \frac{1}{(X - \xi)^2(Y - \psi)^2 \langle F \rangle^4} \\ &\left\{ \sum_{i=1}^{X-\xi} \sum_{j=1}^{Y-\psi} \sum_{k=1}^{X-\xi} \sum_{l=1}^{Y-\psi} M \langle p(i, j) p(i + \xi, j + \psi) p(k, l) p(k + \xi, l + \psi) \rangle + \right. \\ &\quad \left. + \sum_{(k, l) \neq (i, j)} N^2 q^4 \gamma_2^2 g_1(k - i, l - j)^2 + \right. \\ &+ \sum_{(k, l) \neq (i + \xi, j + \psi)} N^2 q^4 \gamma_2^2 g_1(k + \xi - i, l + \psi - j) g_1(k - \xi - i, l - \psi - j) \\ &\quad \left. + \sum_{(i, j) \neq (k + \xi, l + \psi)} N^2 q^4 \gamma_2^2 g_1(k + \xi - i, l + \psi - j) g_1(k - \xi - i, l - \psi - j) \right. \\ &\quad \left. + (X - \xi)(Y - \psi) \left[\langle F \rangle \left(q \frac{\gamma_2}{\gamma_1} + 1 \right) \right]^2 \right. \\ &\quad \left. + 2(X - \xi)(Y - \psi) N q^2 \gamma_2 g_1(2\xi, 2\psi) \left[\langle F \rangle \left(q \frac{\gamma_2}{\gamma_1} + 1 \right) \right] \right\}. \end{aligned} \quad (6)$$

Here, M is the number of particles in the sample volume V , q is the molecular brightness (the average number of detected photons per particle per dwell time), $g_1(\xi, \psi) = N g_D(\xi, \psi)$ is the normalized correlation function for diffusion, $\gamma_k = (\int I^k(\mathbf{r}) d\mathbf{r} / \Omega) = (1/2k\sqrt{2k})$ is the normalized k -th moment of the laser intensity profile with $\Omega = \pi^{(3/2)} w^3 \alpha$ corresponding to the observation volume per position of the laser, and $p(i, j)$ is the detected photon count at pixel (i, j) in the image emitted from a single particle. The moments of p can be expressed in terms of higher-order correlation functions for diffusion; see Eqs. S29–S31 and (9). In particular, the contribution of shot noise, the unavoidable noise caused by the stochastic nature of the photon detection (19), is presented in the last two lines of Eq. 6. Fig. S6 shows that the simulation- or experiment-based and theoretical variances of $G(\xi, \psi)$ are very similar. We conclude that at least for the typical parameter values used, Eq. 6 can accurately predict the variance of the empirical correlation function. A generalization of Eq. 6 to the case in which background noise and dark current contributions are included is discussed in the [Supporting Materials and Methods](#), Eq. S35.

Mean-squared relative error

Let the true diffusion coefficient be D_0 and let $(\hat{D}_1, \dots, \hat{D}_n)$ be a sample of the estimated diffusion coefficients by using RICS in n repetitions of the same experiment or molecular Monte Carlo simulation. Let $(\tau_p, \tau_s, S, w, \alpha, N, \lambda, I_0, X, Y)$ be the set of molecular and instrumental parameters, in which the image size is $X \times Y$ pixels and λ accounts for the photon yield of the particles per unit of time, the absorption coefficient, and the detection efficiency. To evaluate the performance of RICS, we define the mean-squared relative error (MSRE) as

$$\text{MSRE} = \frac{1}{n} \sum_{k=1}^n \left(\frac{\hat{D}_k - D_0}{D_0} \right)^2, \quad (7)$$

which depends on the molecular and instrumental parameters. In general, a systematic deviation of the estimated diffusion coefficient or an increased variance would lead to a larger value of the MSRE. When comparing

two sets of experimental settings, one should prefer the one with a smaller MSRE. Together with the MSRE, we consider the kernel density estimate of the probability density $P(D|D_0)$ for the sample $(\hat{D}_1, \dots, \hat{D}_n)$. Intuitively, $P(D|D_0)dx$ describes the probability of obtaining an estimate of the diffusion coefficient in the infinitesimal interval $[D, D + dx]$ when the true value is D_0 . The kernel density estimation (20) is a standard nonparametric method to estimate the probability density function, providing a visualization of the properties of a sample and simpler interpretation of the value of the MSRE; see Fig. 1. The bandwidth h in the kernel density estimator is chosen according to Scott's rule, i.e., $h = (4\sigma^5/3n)^{(1/5)}$, where σ is the SD of the sample and n the sample size; see (20). As an example, in Fig. 1, kernel density estimates of the estimated diffusion coefficients are presented for a wide range of typical values of the pixel dwell time. To produce the kernel density estimates we use the estimated values for the diffusion coefficient obtained by RICSPE, see RICSPE below. The MSRE corresponding to the samples underlying the densities shown is reported in the insert to Fig. 1 and will be used to measure the goodness of the experimental setting.

RICSPE

In this section, we introduce an alternative method to the experiments and molecular Monte Carlo simulations used throughout the [Results](#) to generate a sample of estimated diffusion coefficients $(\hat{D}_1, \dots, \hat{D}_n)$. We call this method, described in detail in steps 1 and 2 below, RICSPE. RICS analysis assumes that the observed empirical correlation function $G(\xi, \psi)$ provides an estimate of the infinite time limit $g_{D_0}(\xi, \psi)$ up to measurement errors. Mathematically, this can be formulated as

$$\vec{\epsilon} = [G(\xi, \psi) - g_{D_0}(\xi, \psi)] + \epsilon(\xi, \psi), \quad (8)$$

$$\vec{\epsilon} = [\epsilon(\xi_1, \psi_1), \dots, \epsilon(\xi_{\max}, \psi_{\max})] \sim N(0, \Sigma),$$

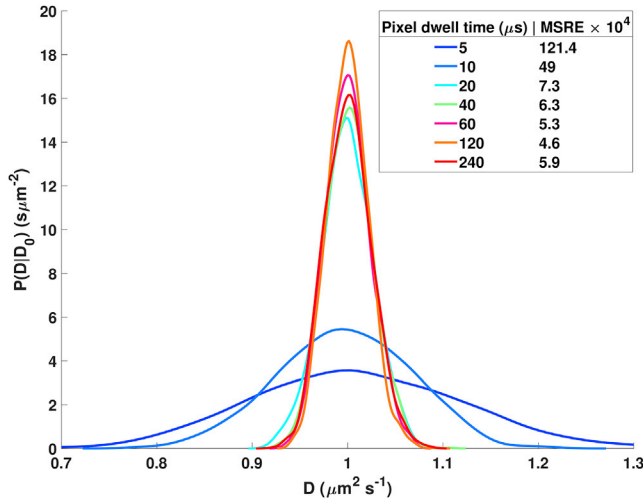


FIGURE 1 The kernel density estimate of the probability density $P(D|D_0 = 1)$ for different pixel dwell times τ_p and $\tau_l = 200\tau_p$ when $D_0 = 1 \mu\text{m}^2 \text{s}^{-1}$, $S = 0.05 \mu\text{m}$, $w = 0.2 \mu\text{m}$, $\alpha = 5$, $X = Y = 200$, $N = 1.74$, and $\lambda I_0 = 1000 \text{ kHz}$. Each sample contains 2000 observations, and each observation is obtained by fitting the mean ACF of a stack of 20 frames. The different colors correspond to different pixel dwell times. To see this figure in color, go online.

where $\vec{\epsilon} \sim N(0, \Sigma)$ indicates that $\vec{\epsilon}$ follows a multivariate normal distribution with covariance matrix Σ and ξ_{\max} and ψ_{\max} are the maximal spatial lags considered. The diffusion coefficient estimate is then the minimizer of the weighted sum of squared residuals

$$\hat{D} = \underset{D}{\operatorname{argmin}} \sum_{\xi, \psi} \left(\frac{G(\xi, \psi) - g_D(\xi, \psi)}{\sigma(\xi, \psi)} \right)^2, \quad (9)$$

where $\sigma(\xi, \psi) = \sqrt{\operatorname{Var}[G(\xi, \psi)]}$. In the next section, we present an analytic formula to compute the elements of Σ ; see Eqs. 6 and S24. Let us now fix the number of repetitions N_{rep} of the simulation. The number of images in one simulation, N_{frames} , varies from dozens to hundreds of images. We can generate samples of estimated diffusion coefficients $(\hat{D}_1, \dots, \hat{D}_{N_{\text{rep}}})$ as follows:

- 1) For the lags considered, compute Σ according to Eqs. 6 and S24. Draw independent $\vec{\epsilon}_k \sim N(0, \Sigma)$ for $k = 1, \dots, N_{\text{rep}}$.
- 2) Compute $G_k(\xi, \psi) = g_{D_0}(\xi, \psi) + E_k(\xi, \psi)$ for each ξ and ψ and perform a least-squares fit to obtain

$$\hat{D}_k = \underset{D}{\operatorname{argmin}} \sum_{\xi, \psi} \left(\frac{G_k(\xi, \psi) - g_D(\xi, \psi)}{\sigma(\xi, \psi)} \right)^2, \quad (10)$$

as done in RICS.

Because the correlation function is almost symmetric, we fit only the positive quadrant of it. The MSRE is called empirical MSRE if the sample $(\hat{D}_1, \dots, \hat{D}_n)$ comes from n repetitions of the same molecular Monte Carlo simulation and theoretical MSRE if the sample $(\hat{D}_1, \dots, \hat{D}_n)$ is obtained by RICSPE.

Computer programs and molecular Monte Carlo simulations

In the main simulation study, particle trajectories were simulated using Gaussian random walk (discrete-time Brownian motion) in a box. The pa-

rameters in the simulations were kept close to the experimental settings, except for the brightness in some simulations. Typical values for the brightness in experiments are between 5 and 300 kHz; however, we sometimes used a value of 1000 kHz to reduce the computational cost of the simulations because we could, in this way, achieve the same average signal with a lower number of simulated particles. In the analysis, the measurement time does not include time lost because of retracing the laser beam between consecutive images. The time the beam is moving without scanning depends on the microscope manufacturer. The analysis we performed can be adjusted to the microscope specifications. There are many parameters involved, and the values are specified later case by case. The side of the box was extended by at least $2 \mu\text{m}$ on each side of the image, and periodic boundary conditions were used to avoid edge effects. All simulations were performed using the software Pulsed Interleaved Excitation Analysis with MATLAB (PAM) (21). The PAM software generates RICS data by simulating the diffusion of the particles combined with the raster scan of the laser beam at a certain scan speed. More information about the software PAM, together with its manual, can be found at <https://pam.readthedocs.io/en/latest/>. The PAM software was also used to analyze experimental data. The experimental images are preprocessed with a moving average to remove possible artifacts and inhomogeneities. In the moving average, each frame is averaged with the previous and subsequent two frames. From the preprocessed images, the mean ACF is computed, and parameter estimates are obtained by nonlinear least-square fitting of the theoretical model in Eq. 3, in which an offset is included to correct for a possible baseline of the ACF. We consider 20 lags in each direction when fitting the correlation function, and, as is typically done in RICS experiments, $G(0, 0)$ is not used in the fit because it is corrupted by shot noise. For the experiments, two types of confidence intervals for the diffusion coefficient are reported: least-squares confidence intervals obtained from the residuals of the least-squares fitting and bootstrap confidence intervals obtained by resampling a stack of images. More details can be found in Confidence Intervals below. Both the source code and a GUI to run the RICSPE method are available at <https://gitlab.com/PAM-PIE/PAM> or at <https://gitlab.com/Longfils/raster-image-correlation-spectroscopy-performance-evaluation>. A brief description of the GUI is presented in the Supporting Materials and Methods. The analysis and simulations were performed on a computer with an Intel i7-5600 dual-core processor running at 2.6 GHz using 16 Gb of random-access memory.

Bootstrap

The bootstrap technique (22) can be used to obtain estimates of bias and SD of the diffusion coefficient estimated by RICS. Typically, one RICS experiment comprises a series of frames. In our simulations and experiments, the number of frames N_{frames} varies between 20 and 400. The bootstrap method consists of drawing the same number N_{frames} of images with replacement from the original set of images and estimating the diffusion coefficient by using RICS based on this new sample. The sampling procedure is repeated N_{boot} times, where N_{boot} is between 50 and 250, leading to N_{boot} estimates of the diffusion coefficient, namely $D_1, \dots, D_{N_{\text{boot}}}$. The empirical MSRE of a simulation can be computed by replacing n by N_{boot} and $\hat{D}_1, \dots, \hat{D}_n$ by $D_1, \dots, D_{N_{\text{boot}}}$ in Eq. 7.

Confidence intervals

In this manuscript, we use two types of confidence intervals, which we call least-squares confidence intervals and bootstrap confidence intervals. The former ones are defined as the approximate confidence region of the nonlinear model, the RICS ACF, in which the nonlinearity is partially taken into account by considering the Jacobian matrix evaluated at the minimizer of the least squares (23). Moreover, the confidence region as constructed from the Jacobian are symmetric, whereas in general, the confidence regions for nonlinear models are not. The latter ones are obtained by

bootstrapping the stack of images as follows: suppose we have a series of N_{frames} images. We can draw a new stack of images by drawing N_{frames} images with replacements from the original stack of frames. In such a way, we can generate a number N_{boot} of stacks and estimate the diffusion coefficient from each one of them. This procedure leads to a sample $D_1, \dots, D_{N_{\text{boot}}}$ that can be used to estimate the variability of the diffusion coefficient estimate; see (24) for more details.

Experiments

Before imaging, an eight-well chambered coverslip (Lab-Tek Chambered Cover glass; Thermo Fisher Scientific, Waltham, MA) was incubated for 30 min with 1 mg/mL bovine serum albumin (Sigma-Aldrich, Overijse, Belgium) to prevent nonspecific adhesion of the dye and washed twice with the measurement buffer. Depending on the experiment, the dye was Atto488-COOH (ATTO-TEC, Siegen, Germany) diluted in phosphate-buffered saline (PBS), enhanced green fluorescent protein (eGFP) dissolved in PBS, or eGFP dissolved in PBS buffer containing 46% (w/w) sucrose (VWR, Leuven, Belgium) with a viscosity of $10.28 \text{ mPa} \cdot \text{s}$ at 20°C . Two microscopes were used for the RICS experiments. The commercial instrument was a Zeiss LSM880 confocal laser scanning microscope (Carl Zeiss, Jena, Germany) equipped with a Zeiss C-Apochromat $63\times/1.2 \text{ W}$ Korr objective. Atto488-COOH and eGFP were excited with a 488 nm Ar-ion laser (3.6 μW in the sample, S170C microscope slide power sensor; Thorlabs, Munich, Germany). An MBS488 dichroic mirror was used. Emitted light was registered between 489 and 695 nm using the Zeiss Quasar GaAsP detector operated in photon-counting mode. Pixel size was constant at 50 nm, with an image resolution of 256 by 256 pixels (digital zoom 10.5, image size 12.85 by 12.85 μm). For each measurement, between 20 and 400 frames were acquired at 10 μm above the coverslip with a varying pixel dwell time and line time, as specified in the Results. The custom microscope was built around an inverted microscope (IX71; Olympus Belgium, Berchem, Belgium). A galvanometric mirror scanner (TILL Yanus IV digital scanner; FEI Munich, Gräfelfing, Germany) was used to generate raster-scanned images. Here, a 485 nm laser diode (LDH-D-C-485; Picoquant, Berlin, Germany) pulsing at 20 MHz (PDL 828 Sepia2; Picoquant) was cleaned up with a bandpass filter (Chroma ET485/20 \times , F49-482; AHF Analysentechnik, Tübingen, Germany). Next, the laser was coupled into a single-mode polarization maintaining optical fiber (PMC-400Si-2.6-NA012-3-APB-150-P; Schäfter+Kirchhoff, Hamburg, Germany) using a 60FC-4- RGBV11-47 fiber coupler (Schäfter+Kirchhoff). Light was collimated using a collimator with xyz adjustable lens (60FC-L-4-RGBV11-47; Schäfter+Kirchhoff), the linear polarization was cleaned up (CCM1- PBS251; Thorlabs, Dachau, Germany), and light was reflected via a 3-mm-thick polychroic mirror (Chroma zt405/488/561/640rpc, F73-410; AHF Analysentechnik) into the microscope's back port through the galvo. Imaging was controlled via in-house-developed software (C#; Microsoft Visual Studio). Inside the microscope body, the light was reflected upwards (3-mm-thick Full Reflective Ag Mirror, F21-005; AHF Analysentechnik, mounted in a total internal reflection fluorescence Filter Cube for BX2/IX2, F91-960; AHF Analysentechnik) to the objective lens (UPLSAPO-60XW; Olympus). Sample emission transmitted through the polychroic mirror was focused through a 50 μm pinhole (P50S; Thorlabs) via an achromatic lens (AC254-150-A-ML; Thorlabs) and collimated again (AC254-50-A-ML; Thorlabs). Next, the emission was reflected on (H560LPXR, F48-559; AHF) and transmitted through (H507LPXR, F48-507) two dichroic mirrors, and emission was filtered (HQ 525/50; Chroma) and focused (AC254- 50-A-ML; Thorlabs) on an avalanche photodiode (τ -SPAD; Picoquant). The detector was connected to a time-correlated single-photon-counting device (HydraHarp 400; Picoquant) and powered using a power supply (DSN-102; Picoquant). The laser power was 5 μW for both eGFP and Atto488 data sets, measured between the polychroic mirror and the galvo (LabMax Top, Coherent, Santa Clara, CA), $\sim 40\%$ reached the sample. Again, for each measurement, between 20 and 400 frames

were acquired at 10 μm above the coverslip. The scanned area was 200 by 200 pixels at a pixel size of 48 nm.

RESULTS

We present the results obtained from both simulations and experiments, validating the theory developed for the statistical properties of the empirical ACF. In [Theoretical against Empirical MSRE](#), we show that the theoretical MSRE, obtained by RICSPE, provides a good approximation of the empirical MSRE, obtained by molecular Monte Carlo simulations. Next, we investigate the effects of the different imaging conditions on the estimation of the diffusion coefficient. We complement the simulation study with in vitro experiments of eGFP at different buffer viscosities and summarize our findings in [Tables 2 and 3](#). Last, we examine the confidence intervals for the diffusion coefficient.

Theoretical against empirical MSRE

In [Theory](#), we defined the MSRE (see [Eq. 7](#)) as a measure to evaluate the performance of RICS as a function of the molecular and instrumental parameters. The MSRE captures information about the precision and accuracy of a sample \hat{D}_k , $k = 1, \dots, n$ of estimated diffusion coefficients. The MSRE can be calculated from n repetitions of the same molecular Monte Carlo simulation or experiment, and we refer in this case to the MSRE as empirical MSRE. However, evaluating the performance of RICS via the empirical MSRE is time-consuming. We introduced the RICSPE method to obtain the theoretical MSRE, which allows us to make inferences about the effect of the different experimental parameters on the RICS analysis. We start by studying the relationship between the theoretical and empirical MSRE to verify that the theoretical MSRE can be used in place of the empirical one to estimate the optimal imaging settings for RICS. In [Fig. 2 A](#), the MSREs from repeated molecular Monte Carlo simulations, from bootstrap of the same simulations, and from RICSPE are shown for different pixel dwell times and under the same conditions as the ones used in [Fig. 1](#). Here, τ_l is equal to $200 \tau_p$. The kernel density estimates corresponding to [Fig. 2 A](#) are shown in [Fig. 2, B and C](#) for the cases characterized by $\tau_p = 5 \mu\text{s}$ and $\tau_p = 120 \mu\text{s}$, respectively. The distributions, obtained by RICSPE (*black*) or by repetitions of the same molecular Monte Carlo simulation (*blue*), are close to each other, indicating that the RICSPE method can be used to estimate the distribution of the estimated diffusion coefficient. We conclude that the theoretical MSRE provides a good approximation of the empirical MSRE. Moreover, [Fig. 2 C](#) shows that the distribution of the estimated diffusion coefficient becomes narrower for the optimal pixel dwell time ($\tau_p = 120 \mu\text{s}$) as compared to the suboptimal case in [Fig. 2 B](#) ($\tau_p = 5 \mu\text{s}$). Lastly, in [Fig. 2 D](#), we show the potential of RICSPE by

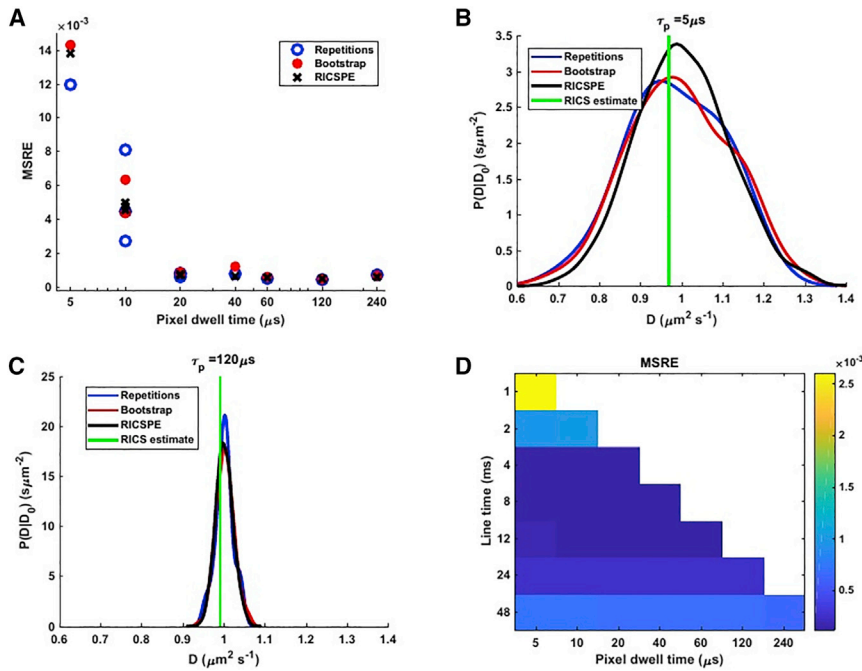


FIGURE 2 (A) Comparison of the theoretical MSRE (black cross) and the empirical MSRE obtained from 20 repetitions of the same simulation (blue circle) and by bootstrapping the simulation (red dot) as a function of the pixel dwell time. The line time is given by $\tau_l = 200\tau_p$. Here, $X = Y = 200$, $S = 0.05 \mu\text{m}$, $w = 0.2$, $\alpha = 5$, $N = 1.74$, $\lambda I_0 = 1000 \text{ kHz}$, and $D = 1 \mu\text{m}^2 \text{ s}^{-1}$. Each molecular Monte Carlo or RICSPE simulation consists of 20 frames. Each simulation has been bootstrapped 250 times, and the number of samples generated by RICSPE is $N_{\text{rep}} = 2000$. (B) A comparison of the kernel density estimates of the diffusion coefficient obtained by RICSPE (black) from $n = 20$ repetitions of the same molecular Monte Carlo simulation (blue) and by bootstrapping the simulation (red) corresponding to the MSRE in (A) with $\tau_p = 5 \mu\text{s}$. An example of the diffusion coefficient estimate provided by RICS is plotted in green. (C) Comparison of the kernel density estimates of the diffusion coefficient obtained by RICSPE (black) from $n = 20$ repetitions of the same molecular Monte Carlo simulation (blue) and by bootstrapping the simulation (red) corresponding to the MSRE in (A) with $\tau_p = 120 \mu\text{s}$. An example of the diffusion coefficient estimate provided by RICS is plotted in green. (D) A comparison of the MSRE for different scan speeds. Each simulation consists of the minimum of 100 frames and the number of frames that can be collected during 3 min, whereas all the other parameters are equal to those in (A). The white color corresponds to physically impossible settings because the time between two consecutive lines here is strictly smaller than the time to scan one line. To see this figure in color, go online.

comparison of the theoretical MSRE for different scan speeds. Each simulation consists of the minimum of 100 frames and the number of frames that can be collected during 3 min, whereas all the other parameters are equal to those in (A). The white color corresponds to physically impossible settings because the time between two consecutive lines here is strictly smaller than the time to scan one line. To see this figure in color, go online.

comparing the MSRE of a wide range of combinations of pixel dwell times and line times.

Because many parameters are involved in the calculation of the experimental correlation function, we now investigate how changing the values of these parameters affects the determination of the diffusion coefficient.

Effect of the scan speed

In general, the ACF in RICS lies between two extreme cases, each of which brings little information about diffusion. The first extreme case is when the scan speed is too slow compared to the movement of the particles and the ACF decays to zero immediately; see Fig. 3 A. The second extreme case is when the scan speed is too fast compared to the movement of the probes and the shape of the ACF resembles the one of the PSF; see Fig. 3 B. In these two extreme cases, the MSRE will likely be high because the ACF holds little information about diffusion. Fig. 3 C shows the behavior of the MSRE as a function of the pixel dwell time when 100 frames are collected. For $D = 1 \mu\text{m}^2 \text{ s}^{-1}$ (see Fig. 3 C), the scan speed giving the minimal MSRE is achieved for a pixel dwell time of $120 \mu\text{s}$ and a line time of 24 ms. In Fig. 1, the probability distribution of the estimated diffusion coefficient computed by RICSPE is plotted as a function of pixel dwell time. We note that for a fixed number of frames per experiment, any pixel dwell time equal to or longer than $20 \mu\text{s}$ leads to comparable results. For $D = 1 \mu\text{m}^2 \text{ s}^{-1}$, there is approximately a factor

of 25 between the MSRE for a simulation with pixel dwell time of $5 \mu\text{s}$ and a line time of 1 ms and the optimal scan speed characterized by a pixel dwell time of $120 \mu\text{s}$ and a line time of 24 ms. The effect of the scan speed for $D = 0.1, 10, 100, 400 \mu\text{m}^2 \text{ s}^{-1}$ is described in detail in the Supporting Materials and Methods.

Although on many microscopes, the pixel dwell time and line time cannot be chosen independently, we can still perform simulations with different combinations to see if it is advantageous for RICS. In Fig. 2 D, we compare many pairs of pixel dwell times and line times. We consider here a measurement time of 3 min and a maximum of 100 frames. We note that the MSRE is almost constant on each row because changing the pixel dwell time does not influence the estimation of the diffusion coefficient. In Fig. 3 B, the infinite time 2D ACF is shown for $\tau_p = 240 \mu\text{s}$ and $\tau_l = 48 \text{ ms}$, where the red lines highlight the cross sections of the 2D ACF in the x - and y -direction. Fig. 3 E shows that all values of the pixel dwell time considered give an ACF in the x -direction that is barely distinguishable from the PSF. Again, for the y -direction, we observe that the MSRE is smallest when the ACF is significantly different from the PSF and the zero ACF, i.e., for line times of 4–8 ms, as shown in Fig. 3 F.

The effect of the scan speed for a fixed measurement time, which limits the number of images we can collect, is studied in detail in the Supporting Materials and Methods; see Fig. S8. Here, we do not include the dark time at the beginning and end of each line in the measurement time. The

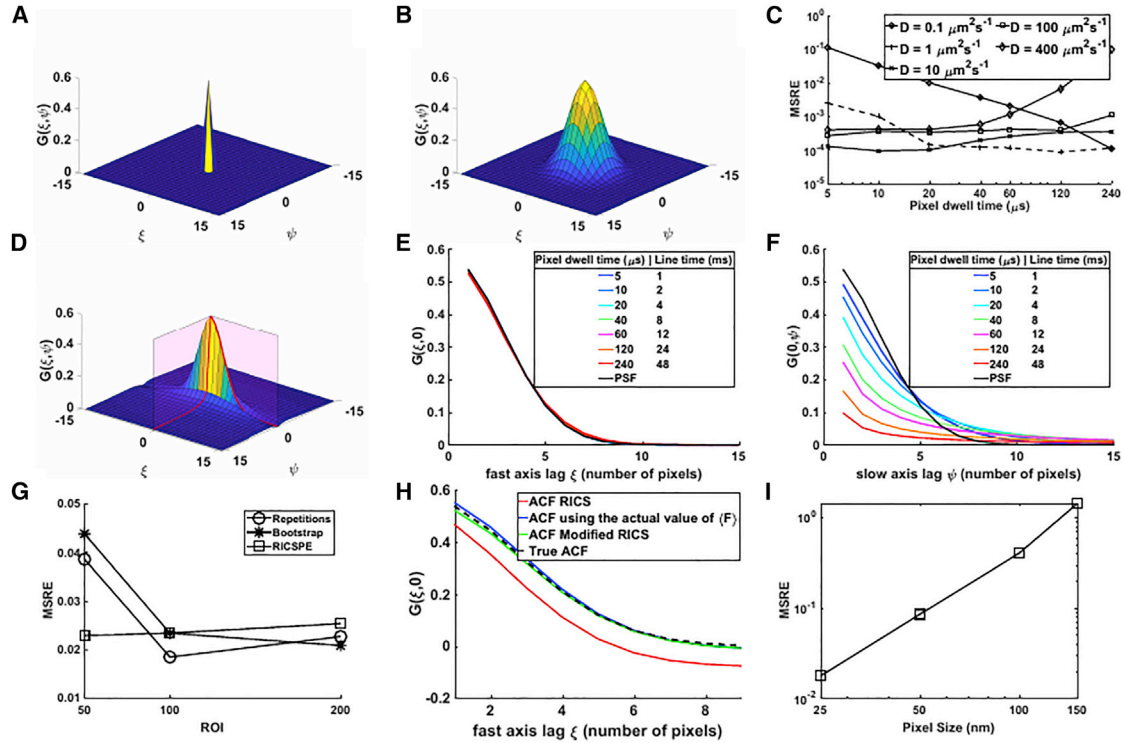


FIGURE 3 (A) Infinite time 2D ACF $G(\xi, \psi)$ when the scan speed is too slow compared to the movement of the particles; (B) infinite time 2D ACF $G(\xi, \psi)$ when the fast scan speed is too fast compared to the movement of the particles; (C) and theoretical MSRE for different scan speeds and diffusion coefficients. The parameters used in this case are $X = Y = 200$, $S = 0.05 \mu\text{m}$, $w = 0.2$, $\alpha = 5$, $N = 1.74$, $\lambda I_0 = 1000 \text{ kHz}$, and $\tau_p = 200\tau_l$. The number of samples generated by RICSPE is $N_{\text{rep}} = 2000$, and each simulation consists of 100 frames; (D) infinite time 2D ACF $G(\xi, \psi)$ for $D = 1 \mu\text{m}^2 \text{ s}^{-1}$, $X = Y = 200$, $S = 0.05 \mu\text{m}$, $\tau_p = 240 \mu\text{s}$, $\tau_l = 48 \text{ ms}$, $w = 0.2$, $\alpha = 5$, and $N = 1.74$. The red lines represent the cross sections $G(\xi, 0)$ and $G(0, \psi)$ in the x - and y -directions, respectively. (E) A cross section $G(\xi, 0)$ of the infinite time ACF in the x -direction for different combinations of pixel dwell time and line time. The legend reports the pixel dwell time in μs and the line time in ms of each curve. The parameters used in this case are the same as in (B) except for τ_p and τ_l . (F) Cross section $G(0, \psi)$ of the infinite time ACF in the y -direction for different combinations of pixel dwell time and line time. The legend reports the pixel dwell time in μs and the line time in ms of each curve. The parameters used in this case are the same as in (D) except for τ_p and τ_l . (G) MSRE as a function of the size $X = Y$ of the ROI for a fixed number of pixels scanned. Here, the parameters are the same as in (A) except that $\tau_p = 5 \mu\text{s}$, $\tau_l = 1 \text{ ms}$ and we consider four 200×200 pixels frames, sixteen 100×100 pixels frames, and sixty-four 50×50 pixels frames, equivalent to a total of 1.6×10^5 pixels scanned and corresponding measurement times of 0.8, 1.6, and 3.2 s. Each simulation consists of N_{frames} frames and has been bootstrapped 250 times. (H) Cross sections of the ACF in the x -direction computed in different ways for 20×20 pixels ROI as reported in the legend. Here, $S = 0.05 \mu\text{m}$, $\tau_p = 5 \mu\text{s}$, $\tau_l = 1 \text{ ms}$, $w = 0.2$, $\alpha = 5$, $N = 1.74$, $\lambda I_0 = 1000 \text{ kHz}$, $D = 1 \mu\text{m}^2 \text{ s}^{-1}$, and $N_{\text{frames}} = 400$. (I) Theoretical MSRE as a function of the pixel size. Here, all the parameters except for the pixel size and the scan speed ($\tau_p = 5 \mu\text{s}$, $\tau_l = 1 \text{ ms}$) are the same as in (C). Each simulation consists of $N_{\text{frames}} = 20$ frames. To see this figure in color, go online.

reduced number of images collected worsens the performance of scan speed with a pixel dwell time longer than $40 \mu\text{s}$ irrespective of the value of the diffusion coefficient.

Effect of the size of the ROI

To study the effect of a larger ROI size, it is important to decrease the number of frames pro rata so as to keep the total number of analyzed pixels constant. When doing this, increasing the ROI size does not significantly improve the MSRE (Fig. 3 G).

Considering a small ROI could be beneficial if it gives access to a better combination of pixel dwell time and line time for a particular value of the diffusion coefficient. Otherwise, large ROIs are advantageous, as previously demonstrated in (5,6). In experiments, often one would like to map the diffusion coefficient locally by repeating

the RICS analysis on small regions (18,25). For very small regions, of size at most 50×50 pixels, the estimated ACF deviates considerably from the infinite time limit ACF (18) because of the estimation bias; see Fig. 3 H (red line). We demonstrate here and in the section “Bias of the ACF: dependence and estimation biases” in the Supporting Materials and Methods that the observed bias is caused by the estimation of $\langle F \rangle$ by $(1/XY) \sum_{i=1}^X \sum_{j=1}^Y F(i, j)$. In fact, when we estimate the ACF using the true value of $\langle F \rangle$, we do not observe any deviation from the infinite time limit ACF for any ROI size ($\geq 6 \times 6$ pixels or $300 \times 300 \text{ nm}$); see Fig. 3 H (blue line) and Fig. S4, C and D. To correctly retrieve information about diffusion for small regions, we propose a simple method (modified RICS) to correct for the estimation bias in the section “Bias of the ACF: dependence and estimation biases” in the Supporting Materials and Methods. Fig. 3 H (green line) shows that the modified

RICS analysis eliminates the bias in the estimated ACF. In Fig. S4, we show that the modified RICS analysis corrects for the bias for ROIs as small as 6×6 pixels. Finally, in Fig. S5, we compare the estimated diffusion coefficient based on the standard RICS analysis (Fig. S5 A) and the estimate based on the modified RICS analysis (Fig. S5 B). It is clear that the proposed method provides more accurate estimates for the diffusion coefficient for small ROIs.

Effect of the pixel size

Pixel size is an important parameter when performing an RICS experiment. The spatial correlation term in the ACF is introduced when the pixel size is smaller than the diameter of the PSF. We recall that the waist of the observation volume is denoted by w , and here, $w = 0.2 \mu\text{m}$. Furthermore, the observation volume is microscope-dependent, and it must be calibrated before performing the experiment. In Fig. 3 F, we can see that the MSRE grows exponentially as a function of pixel size and that halving the pixel size reduces the MSRE by approximately a factor of 5 for $D = 1 \mu\text{m}^2 \text{s}^{-1}$ and by approximately a factor of 3 for $D = 10 \mu\text{m}^2 \text{s}^{-1}$ (data not shown). In particular, pixel sizes larger than 100 nm or for the general microscope sizes larger than $(w/2)$ should be avoided. At the same time, decreasing the pixel size while all the other parameters are kept constant has the effect of decreasing the total region scanned, which could lead to larger artifacts because of effects such as photobleaching. The pixel size 100 nm could be used if the number of frames in the simulation or experiment is 100 or more. The larger pixel sizes lead to an ACF that will be nonzero only at short lags. For example, consider the case in which the value of the ACF at lag (9, 0) is

10% of its amplitude, i.e., $G(9, 0) = 0.1G(0, 0)$, with a pixel size of 50 nm. Then, if we would consider the same experiment but with a pixel size of 150 nm, the value of the ACF will be 10% of its amplitude at lag (3, 0), i.e., $G(3, 0) = 0.1G(0, 0)$.

Effect of the brightness

In Figs. 4 A and S15, the MSRE does not change significantly when the brightness is greater than 100 kHz, and we conclude that the brightness plays a role in the estimation of the diffusion coefficient only if the count per particle per second is low (<100 kHz). In Fig. S15, we can notice that the MSRE increases steeply when the brightness changes from 10 to 1 kHz. We recommend having the average photon count E per particle per second larger than 5 kHz or an average pixel intensity greater than 0.03 counts per pixel. If this is not possible, we suggest increasing the number of frames in the image series and therefore the total measurement time. For example, comparing the MSRE values in Figs. 4 A and S15 for the case $\epsilon = 10$ kHz, we can see that the MSRE is ~ 0.08 when the number of frames is 20 (Fig. 4 A) and ~ 0.02 when the number of frames is 100 (Fig. S15), given that all the other parameters are fixed. The measurement time should be chosen so that the experiment is not affected by photobleaching or small drift.

Effect of the concentration

The concentration of particles in RICS experiments typically ranges between 1 nM and 1 μM . We observe (see Fig. 4 B) that when the concentration is of the order

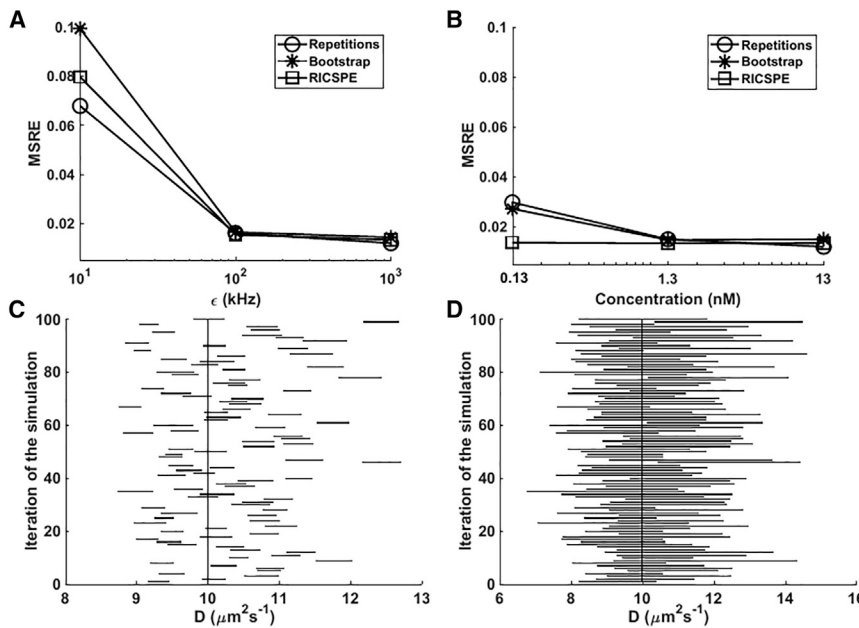


FIGURE 4 Comparison of the theoretical MSRE (square) and the empirical MSRE obtained from 20 repetitions of the same simulation (star) and by bootstrapping the simulation (circle). The common parameters used in the two panels are $X = Y = 200$, $S = 0.05 \mu\text{m}$, $\tau_p = 5 \mu\text{s}$, $\tau_l = 1 \text{ms}$, $w = 0.2 \mu\text{m}$, $\alpha = 5$, $D = 1 \mu\text{m}^2 \text{s}^{-1}$, and $N_{\text{frames}} = 20$. Each simulation has been bootstrapped 250 times, and the number of samples generated by RICSPE is $N_{\text{rep}} = 2000$. (A) MSRE as a function of the brightness λI_0 . Here, $N = 1.74$. (B) MSRE as a function of the concentration with $\lambda I_0 = 1000$ kHz is shown. (C) 95% (nominal value) confidence intervals from the least-square fitting for $X = Y = 200$, $S = 0.05 \mu\text{m}$, $\tau_p = 5 \mu\text{s}$, $\tau_l = 1 \text{ms}$, $w = 0.2 \mu\text{m}$, $\alpha = 5$, $N = 1.74$, $\lambda I_0 = 1000$ kHz, $D = 10 \mu\text{m}^2 \text{s}^{-1}$, and $N_{\text{frames}} = 100$; (D) confidence intervals from bootstrapping from the same simulations as in (C).

0.1 nM, the predicted distribution of the estimated diffusion coefficient by RICSPE deviates from the observed distribution obtained by repetitions of the same molecular Monte Carlo simulation but is of the same magnitude. This is a limitation of RICSPE because it does not capture the effect of very low concentrations (~ 0.1 nM) on the determination of the diffusion coefficient. We have not performed molecular Monte Carlo simulations with concentrations higher than 13 nM because of the computational cost. The MSRE of RICSPE is essentially independent of the concentration of the particles; see Figs. 4 B and S16. Note that the difference in the magnitude of the MSRE is due to the number of ACFs averaged in each repetition of the simulation. In Fig. 4 B, 20 ACFs have been used, and in Fig. S16, 100 ACFs were used. At low concentrations, the background and dark current contributions become relevant. In particular, the fluorescence intensity F can be decomposed as $F = F_p + \text{Noise}$, where F_p denotes the signal from the particles and Noise the contribution of any source of noise uncorrelated with F_p . Then, the denominator in Eq. 4 is incorrect, and one should consider statistical weighting (26,27) to filter out the noise or normalizing the ACF by the square of $\langle F_p \rangle = \langle F \rangle - \langle \text{Noise} \rangle$.

Confidence intervals

It is common practice in RICS to report, together with the point estimate, the confidence interval for the estimated parameters. In particular, the confidence interval can provide information about the variability of the parameter when it is not possible to obtain an estimate of the standard error from repetitions of the same experiment. Although confidence intervals are easily interpreted by the RICS user, they are only approximate confidence intervals, and their confidence level is, in general, not known. Thus, even if in RICS the confidence intervals at given confidence levels are typically considered, the actual confidence level can be much smaller, as the following brief simulation study shows. To investigate the true level for the two types of confidence intervals, least-squares and bootstrap confidence intervals, we repeat the same simulation 100 times and compute the proportion p of the confidence intervals that contain the true value of the diffusion coefficient. We report the results in Figs. 4, C and D and S17 and S18 and Table 1. Even though this simulation study is limited,

it is clear that the least-squares confidence intervals underestimate the variability of the diffusion coefficient. The confidence intervals as obtained by bootstrapping are better, see Table 1, even though we can observe a lower confidence level for the case $D = 1 \mu\text{m}^2 \text{s}^{-1}$ than the claimed 95% level. We observe (see Fig. S17) that the lower confidence level is caused by a tendency to underestimate the diffusion coefficient. Hence, it is preferable to report the bootstrap-based confidence intervals, although care must be taken when the variability of the diffusion coefficient for RICS has not been estimated from repetitions of the same experiment.

Experimental results

We now look at the experiments, in light of the conclusions we have drawn above regarding the effect of the different parameters on the estimated diffusion coefficient. We show one sample frame, the mean ACF, and the weighted residuals of the fitting for one experiment of eGFP in PBS and sucrose for the scan speed characterized by $\tau_p = 16.1 \mu\text{s}$ and $\tau_l = 3.9$ ms; see Fig. 5. In Fig. 5, G and H, the RICS estimates from the experiments with different scan speeds of eGFP in sucrose and PBS are shown. We have three repetitions of each scan speed, and in Fig. 5, G and H, the corresponding estimated diffusion coefficients and their 95% confidence intervals are presented, in which squares indicate confidence intervals obtained from the nonlinear fitting and circles indicate the bootstrap confidence intervals. Note that the stated level of 95% of the confidence intervals does not correspond to the true level. The confidence level is a general issue of nonlinear models. In our case, the confidence intervals, obtained from either the nonlinear fitting procedure or bootstrap, are often too narrow; see Confidence Intervals above. If we extrapolate from the results of the analysis based on simulation (see Fig. 3 A), the optimal combination of pixel dwell time and line time would be $\tau_p = 16.1 \mu\text{s}$ and $\tau_l = 3.9$ ms, respectively. Note that the experiments have been performed with about the same measurement time, implying that the experiments with large pixel dwell time in Fig. 5, G and H are based on a smaller number of frames. According to the recommendations given in the previous sections, for a diffusion coefficient of about $10 \mu\text{m}^2 \text{s}^{-1}$, the optimal results should be obtained with a line time for a fixed measurement time between 1 and 4 ms. In particular, we can observe that in Fig. 5, G and H, the confidence intervals for experiments performed with a long line time are wider than those performed with optimal or close to optimal line time. Similarly, for a diffusion coefficient of about $100 \mu\text{m}^2 \text{s}^{-1}$, the important parameter is the pixel dwell time. In Fig. 5, G and H, the most precise estimates of the diffusion coefficient are obtained with a pixel dwell time of $16 \mu\text{s}$. This result is in agreement with the recommendation of

TABLE 1 Estimated Level for the 95% Confidence Intervals for Different Values of the Diffusion Coefficient

D ($\mu\text{m}^2 \text{s}^{-1}$)	Observed Level of the Least-Squares Confidence Interval (%)	Observed Level of the Bootstrap Confidence Interval (%)
1	11	75
10	15	96
100	27	92

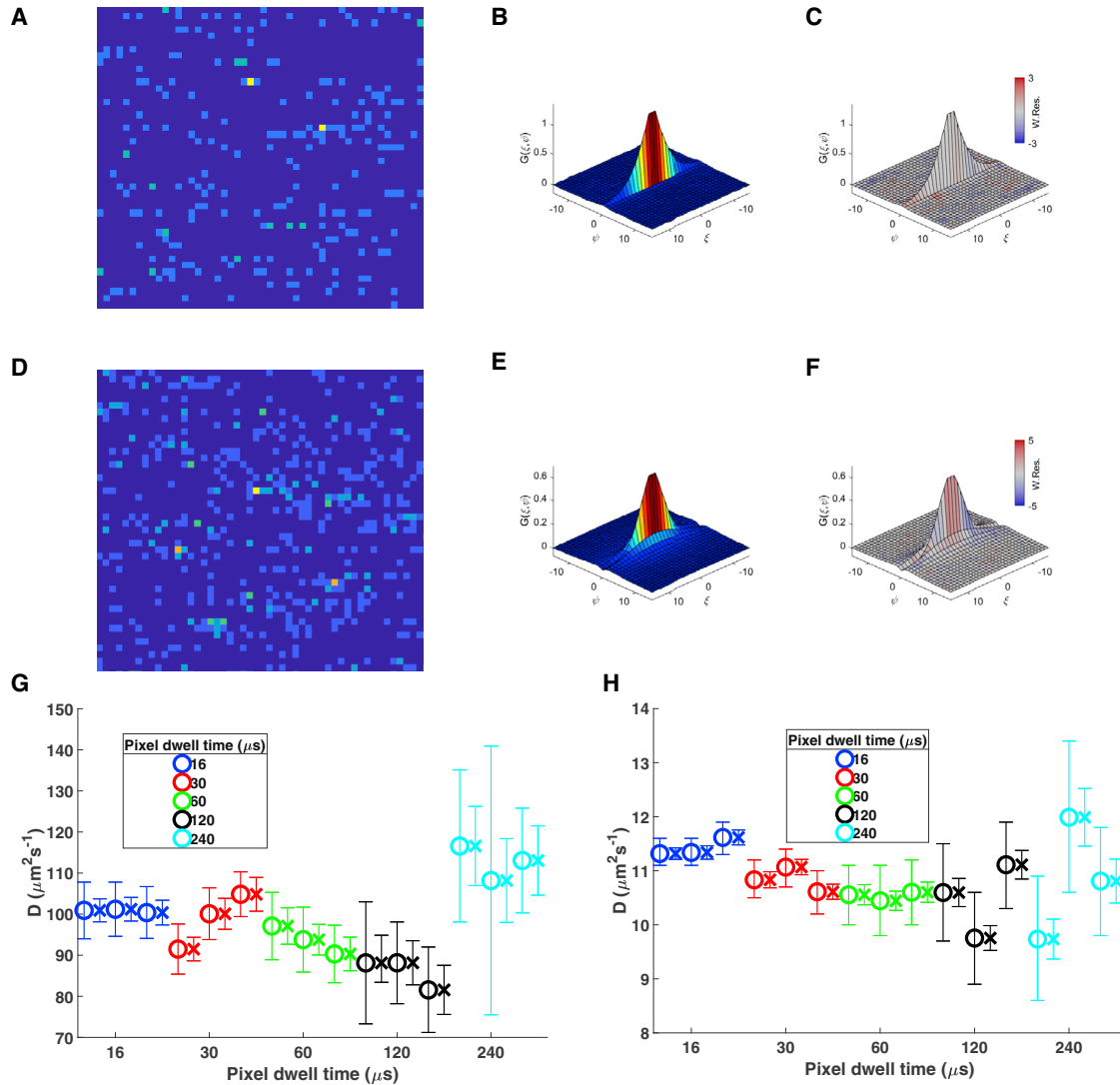


FIGURE 5 (A) Zoomed 40×40 pixels region from a sample frame from the experiment of eGFP in PBS collected with the custom microscope corresponding to the results in the first row of Table S1. The parameters are $X = Y = 200$, $S = 48$ nm, $\tau_p = 16.1$ μ s, $\tau_l = 3.9$ ms, $w = 0.21$ μ m, $\alpha = 4.7$, $N = 0.8$, and $\lambda_0 = 20$ kHz; (B) the mean ACF has been calculated from the stack of images; (C) the mean ACF was fitted and color-coded using the weighted residuals at each lag; (D) zoomed 40×40 pixel region from a sample frame from the experiment of eGFP in sucrose collected with the custom microscope corresponding to the results in the first row of Table S2. The parameters are $X = Y = 200$, $S = 48$ nm, $\tau_p = 16.1$ μ s, $\tau_l = 3.9$ ms, $w = 0.21$ μ m, $\alpha = 4.7$, $N = 0.8$, and $\lambda_0 = 18$ kHz; (E) the mean ACF has been calculated from the stack of images; (F) the mean ACF was fitted and color-coded using the weighted residuals at each lag. (G) Results for repeated experiments of eGFP in PBS for different scan speeds. The same results are shown in Table S1. (H) Results for experiments of eGFP in sucrose for different scan speeds. The same results are shown in Table S2. We present point estimates for the diffusion coefficient and two types of confidence intervals: least-squares confidence intervals (cross) and bootstrap confidence intervals (circle). Observe that the indicated level of 95% of the confidence intervals does not correspond to the true level; see Table 1. The bars have been displaced to avoid overlap, and the correct pixel dwell time is indicated by the color. To see this figure in color, go online.

using in this case a pixel dwell time between 5 and 20 μ s obtained from the simulation study.

DISCUSSION

In this work, we presented analytical formulae for the bias and the variance of the empirical ACF of RICS. The variance for the ACF of RICS derived in this work and the variance for the ACF of FCS (Eq. 21; (11)) show many similarities but also some differences. These differences

prevent extrapolating the published results of FCS to RICS. The comparison of the results obtained from the derived expression for the variance of RICS and the results from experiments and simulations (Figs. S6 and S7) validate the formulae developed in this work. We proposed the MSRE as a measure of the combined effects of accuracy and precision of RICS. The MSRE has the advantage of penalizing equally small absolute deviations below and above the correct value D_0 . Although the MSRE maximal value for large absolute deviations of D below D_0 is 1,

this does not pose a limitation to its usefulness because a value of the MSRE close to 1 is a strong indication that such experimental settings should be avoided. In (12), it was shown that the error of the estimated diffusion coefficient in FCS is a function of $\log(D/D_0)$. Nonetheless, the use of the logarithm of the ratio would penalize more underestimation than overestimation, introducing an asymmetry that we think is not desirable in this context.

We found that the dependence bias of the ACF is negligible for RICS experiments, even for small ROI ($\leq 50 \times 50$ pixels). In particular, increasing the number of collected pixels by changing the size of the ROI and the measurement time made the bias of the ACF presented in Eq. 5 less important. On the other hand, the estimation bias cannot be ignored for ROI of size $\leq 50 \times 50$ pixels. Thus, we proposed the modified RICS analysis to correct for the estimation bias. In actual experiments, other sources of possible bias may occur, such as photobleaching, dye blinking, and sample drift, that we did not consider here. Such bias, as opposed to the bias discussed here in detail, will most likely not become negligible even by sufficient sampling. A possible extension of our work to include the bias because of photobleaching, dye blinking, and sample drift could be used to develop a correction of the bias, for example, by including the bias in the mean of the error terms in Eq. 8. Then, if an approximation of this bias is available, it is straightforward to generate the biased measurement errors from the multivariate normal distribution.

The main advantage of RICSPE compared to the molecular Monte Carlo simulation is that we do not need to simulate raster images, which are more computationally demanding than simulation of the ACFs. For example, to perform one molecular Monte Carlo simulation with the typical settings used in RICS takes approximately 2 h and 20 min. To realistically evaluate the accuracy and precision of the estimated diffusion coefficient, at least 10 repetitions of such a simulation would be required, i.e., more than 20 h total. RICSPE takes, under the same conditions, about 1 h and 40 min. Moreover, RICSPE scales extremely well in the number of repetitions, number of frames in one stack, and concentration. In fact, in RICSPE, we do not simulate diffusing particles, and thus, increasing the concentration does not change the computational cost of the analysis. On the other hand, one molecular Monte Carlo simulation with concentration greater than or equal to 100 nM takes ~ 7 days. Although molecular Monte Carlo simulation time scales linearly in the number of repetitions and frames used, RICSPE has a sublinear scaling because of the fact that most of the time is spent on computing the covariance matrix of the ACF, which is common for all repetitions.

In the Results, we presented recommendations on the choice of the scan speed, pixel size, concentration, brightness, and size of the ROI. Previously published guidelines (6) recommended the use of pixel dwell times in the range of 8–20 μs and to use

$$\tau_p < \frac{w^2}{4D} \quad (11)$$

to obtain a successful RICS experiment. With such pixel dwell time values, the ACF will be nonzero in at least the scanning direction. However, Eq. 11 limits the possible values of the pixel dwell time that can be used in an experiment only when the diffusion coefficient is relatively high ($> 10 \mu\text{m}^2 \text{s}^{-1}$). As an example, let the lateral waist of the PSF be $w = 0.2 \mu\text{m}$. Then, for $D = 0.1 \mu\text{m}^2 \text{s}^{-1}$, the condition in Eq. 11 becomes $\tau_p < 100 \text{ ms}$; for $D = 1 \mu\text{m}^2 \text{s}^{-1}$, it becomes $\tau_p < 10 \text{ ms}$; for $D = 10 \mu\text{m}^2 \text{s}^{-1}$, it becomes $\tau_p < 1 \text{ ms}$; and for $D = 100 \mu\text{m}^2 \text{s}^{-1}$, it becomes $\tau_p < 100 \mu\text{s}$. Our conclusion is that for slowly diffusing particles ($D = 0.1\text{--}1 \mu\text{m}^2 \text{s}^{-1}$), the crucial parameter is the line time rather than the pixel dwell time; see Figs. 3 and S9. The line time depends on the pixel dwell time and the retracing time of the beam, which is dependent on the microscope. Eq. 11 assures that the ACF is nonzero at least for short lags, but one needs a similar bound to guarantee that the correlation function is also distinguishable from the PSF. The RICSPE method provides a practical way to check that the scan speed is neither too fast nor too slow. Furthermore, Eq. 11 does not provide any quantification of the difference in the estimated diffusion coefficient when using two pixel dwell times satisfying the condition in Eq. 11, whereas we show that the MSRE has this potential. For $D = 10 \mu\text{m}^2 \text{s}^{-1}$, RICSPE indicated that, among the cases tested, a line time $\tau_l = 1, 2, 3 \text{ ms}$ would be recommended. Although these recommendations satisfied the condition in Eq. 11 and the pixel dwell times were approximately in the range 8–20 μs as suggested in (6), Fig. S10 showed that most of the information about the dynamics of the particles lies in the y -direction of the ACF. For $D > 10 \mu\text{m}^2 \text{s}^{-1}$, RICSPE recommended using $\tau_p = 5, 10, 20 \mu\text{s}$, in line with the guidelines presented in (6).

We concluded that the RICS autocorrelation function in the case of a single fluorescent species diffusing in a homogeneous medium contains information on diffusion mostly in one of the two directions; see Figs. 3 and S9–S12. However, RICS in general exploits information on different time-scales. For example, if we considered a mixture of particles with different diffusion coefficients or a heterogeneous medium, then the multiple timescales (microseconds between adjacent pixels in the x -direction, milliseconds between adjacent pixels in the y -direction, and seconds between consecutive frames) present in RICS would allow us to study diffusion in such complex diffusion processes. A global analysis of RICS over different scan speeds, called multiple scan speed intensity correlation spectroscopy (msICS) (28), has been developed. The main advantage of msICS over RICS lies in the possibility of applying this method when little a priori information of the diffusion in the sample is available. In such a situation, selecting the correct scan speed would be difficult. However, a proper comparison between msICS and RICS with comparable

experiments, e.g., with a similar total measurement time, has been missing. Our results suggest that there exists an optimal range of scan speeds for RICS depending on the value of the diffusion coefficient. Thus, it is possible that such optimal settings would outperform a global analysis in RICS for a single diffusing species. Nonetheless, the msICS approach exploits a series of scan speeds, allowing the extraction of information on different timescales, which could be desirable when studying mixtures of diffusing species. RICSPE can be generalized to study samples containing two noninteracting species having different diffusion coefficients by considering weighted sums of Eq. 6 with different parameters. RICSPE can in theory be used to find out whether the two diffusion coefficients can be resolved and possibly provide guidelines on the experimental settings for a given mixture of particles. This could be the subject of a future study.

As discussed above, Eq. 11 ensures a nonzero temporal correlation. Similarly, to have spatial correlation between adjacent pixels, it is important that the pixel size is smaller than the radius of the PSF. Previous recommendations for designing an RICS experiment (6) suggest having the pixel size at least four to five times smaller than the radius w of the PSF. We tested the effect of oversampling the PSF, and we find an improvement between using a pixel size smaller than $(w/4)$ as compared to pixel sizes larger than $(w/2)$. In terms of number of images and size of the ROI, we obtained similar results as in (6).

When the RICSPE method introduced here is used, the concentration of particles did not seem to matter as long as we are in the typical range 1 nM–1 μ M of concentrations suitable for RICS. However, with concentrations on the order of 0.1 nM, the RICSPE method underestimated the variability of the estimated diffusion coefficient. Although RICS still provided good estimates of the diffusion coefficient, these estimates started to be less precise compared to the other concentrations considered. Thus, further investigation is needed. Finally, for an RICS experiment on a homogeneous

sample, we recommend choosing the largest number of pixels in a line X and number of lines Y that allow for the optimal combination of pixel dwell time and line time found as described above. In fact, Fig. 3 G showed that for a fixed number of pixels scanned, the ROI did not play a role, but for a fixed measurement time, it did; see Fig. S14. However, when mapping diffusion locally by applying RICS on small regions, we recommend using the correction introduced in modified RICS. Our guidelines are summarized in Tables 2 and 3. When planning an RICS experiment, the parameters that mostly affect the accuracy and precision of RICS are, in descending order of importance, the scan speed, pixel size, brightness, and size of the ROI. In general, if the condition regarding the brightness in Table 2 cannot be met or when locally mapping diffusion by repeating the analysis on small ROIs, the deterioration in the performance of RICS, in terms of the precision and accuracy of the estimated diffusion coefficient, can be compensated for by increasing the number of frames as long as the longer measurement time does not lead to some unwanted effects (such as photobleaching or sample drift).

An analysis similar to the one proposed here for RICS can be carried out for other ICS methods such as TICS, spatio-temporal image correlation spectroscopy (STICS) (29), and pair correlation function (30). The formulae necessary for the analysis presented in this manuscript can be adapted from the ones derived in the Supporting Materials and Methods. We expect the effect of the common parameters on the precision and accuracy of the estimated diffusion coefficient to be similar in all ICS methods. In ICS methods, the sampling time interval, i.e., the time between successive data points, should be adjusted according to the movement of the particles. For example, in RICS, the sampling time interval is characterized by the combination of pixel dwell time and line time, whereas for TICS or STICS, the sampling time corresponds to the time between consecutive frames. We think that corresponding plots as in Fig. 3, E and F for TICS and STICS could provide a powerful

TABLE 2 Summary of the Recommended Range of Values for the Parameters Considered Here

Parameter	Impact	Range of Values	Further Comments
Brightness	medium	10^2 – 10^3 kHz counts per particle per second for solution experiments. 10 kHz counts per particle per second for cell measurements.	If this recommended condition cannot be met, consider increasing the number of frames while avoiding photobleaching and other common problems of long measurement times.
Concentration	low	1 nM–1 μ M	The concentration does not seem to affect the RICS performance, at least not in the concentration range 1–10 nM. Further investigation at high concentrations (>10 nM) is needed.
Fluorescence intensity	medium	Average photons per pixel ≥ 0.03 .	This condition can be met by increasing the brightness (laser power/probe), the concentration, or the pixel dwell time.
ROI	medium	$\geq 200 \times 200$ for RICS or $\geq 16 \times 16$ for local RICS with bias correction (modified RICS).	Recommended to use the largest image size that allows the combination of pixel dwell time and line time reported in Table 3.
Pixel size	high	Pixel size $< (w/4)$.	RICS can provide good results as long as the pixel size is smaller than or equal to $(w/2)$ if at least 100 images are collected. The value of w has to be calibrated for the microscope. This condition and Eq. 11 are sufficient to guarantee a nonzero ACF.
Scan speed	high	See Table 3.	

TABLE 3 Summary of the Optimal Scan Speed for Different Values of the Diffusion Coefficient

D ($\mu\text{m}^2 \text{s}^{-1}$)	Measurement Time = ∞	Measurement Time = 3 Min, Not Taking into Account the “Dead Time” of the Microscope	Comments
0.1	τ_l is 24 or 48 ms	τ_l is 12, 24, or 48 ms	Avoid using line times less than or equal to 2 ms
1	τ_l is 24 or 48 ms	τ_l is 4 or 8 ms	
10	τ_l is 1, 2, or 4 ms	τ_l is 1, 2, or 4 ms	Pixel dwell times of 1 μs could work as well. Avoid using pixel dwell times greater than or equal to 120 μs .
100	τ_p is 5, 10, or 20 μs	τ_p is 5, 10, or 20 μs	
400	τ_p is 5, 10, or 20 μs	τ_p is 5, 10, or 20 μs	

The column with infinite measurement time refers to an experiment in which having a long measurement time is not problematic. The column with limited measurement time does not take into account the time spent on retracing the beam between frames. In case this “dead time” is accounted for, the number of photons collected will decrease accordingly.

tool to qualitatively determine whether a sampling time would allow for correct determination of the parameters. Similarly, as we discussed for RICS, the pixel size may not be crucial as long as the PSF is oversampled by at least a factor of 4. Furthermore, the effect of the concentration of the probe should be the same in RICS, TICS, and STICS. In general, increasing the number of data points sampled, e.g., the number of frames in TICS or the number of frames and the size of the ROI in RICS and STICS, improves the accuracy and precision of the estimated diffusion coefficient, at the cost of a longer measurement time.

The analysis for arbitrary-region RICS (ARICS) (25) is more complex to perform. In fact, ARICS considers ROIs of any shape, and typically, the shape is defined manually or by using a mean filter. However, such ROIs cannot be known before performing an experiment or a simulation. Nonetheless, the general recommendation that a larger ROI provides more precise estimates still holds. We recommend using an ROI that allows sufficient sampling in the direction of the ACF that contains most of the information about the dynamics of the system. We can also conclude that in the case of a heterogeneous sample in which RICS analysis would be done locally in small regions by dividing the image into small nonoverlapping regions, the increase in the error of the estimated diffusion coefficient due to the small ROI could be counterbalanced by increasing the number of frames in the experiment (18) and adopting the correction in modified RICS. Alternatively, local RICS (18) can be used to locally map the diffusion coefficient after a calibration step based on simulated data. To investigate the results of ARICS, we suggest visualizing, together with the diffusion map, a map of the standard errors of the estimated diffusion coefficient computed by bootstrapping the data set.

A typical step in RICS experiments is the preprocessing of the images by means of a moving average to remove spatial inhomogeneities. The number of frames to be averaged should be chosen to be the maximum such that these inhomogeneities do not move significantly during the scanning of the frames. If we average over more frames, we can obtain a better estimate of the spatial inhomogeneities because the fluctuations of the signal due to the dynamics

of the particles cancel out in the moving average procedure as long as they are immobile.

RICS can be used on a confocal laser scanning microscope with analog detection to determine the diffusion coefficient. Nonetheless, a few precautions must be taken. First, analog detectors can introduce unwanted correlations between adjacent pixels in the x -direction, in particular for short pixel dwell times (14). Thus, it is recommended to either avoid using such fast scan speeds or leave out the corrupted points $G(0, \psi)$ of the ACF in the x -direction during the fitting. In terms of the recommendations given here, for slow-diffusing particles $D \leq 1 \mu\text{m}^2 \text{s}^{-1}$, the correlation on the $\xi = 0$ line of the ACF $G(\xi, \psi)$ is not crucial to recover the diffusion coefficient; see Figs. 3 E and S9. However, for fast-diffusing particles ($D \geq 100 \mu\text{m}^2 \text{s}^{-1}$), we recommend using a fast scan speed because it is the x -direction of the ACF that holds information about diffusion; see Figs. S11 and S12. In such a case, we suggest performing a prestudy by collecting images and optically preventing any light from reaching the detector to check the effect of the correlated noise.

CONCLUSIONS

In this work, we propose the RICSPE method as an alternative to molecular Monte Carlo simulations to investigate the effect of different experimental settings on the accuracy and precision of the estimated diffusion coefficient. RICSPE is based on the simulation of autocorrelation functions, from which a sample of the estimated diffusion coefficients can be obtained by mimicking the RICS analysis. To demonstrate the potential of RICSPE, we show the effect, in decreasing order of importance, of the scan speed, pixel size, brightness, the size of the ROI, and concentration on the performance of RICS. We propose a correction for the deviation of the ACF on small regions, which we call modified RICS, that helps in mapping diffusion locally in the sample. Additionally, we advise RICS users to be cautious when reporting confidence intervals for the diffusion coefficient. We provide a GUI to run RICSPE through a repository. We suggest that the RICS user list, for the particular microscope, all the possible combinations of pixel dwell

time and line time for a certain ROI. Then, given an estimate of the magnitude of the diffusion coefficient and the probe brightness obtained either in a prestudy or from the literature, fill in the corresponding fields in the RICSPE GUI. The program will recommend the best combination of pixel dwell time and line time for the experimental condition used as input. Afterwards, if the variability of the diffusion coefficient is still large, one can change the measurement time and the number of frames to check their minimal values to reduce such variability below a predetermined level. We believe that the recommendations presented here could help RICS users in their daily research.

SUPPORTING MATERIAL

Supporting Material can be found online at <https://doi.org/10.1016/j.bpj.2019.09.045>.

AUTHOR CONTRIBUTIONS

M.L. and A.S. developed the theory of the technique. M.L., N.S., M.A., N.L., and J.H. designed the study. N.S., V.L., G.S.F., and J.H. contributed to the design, acquisition, and interpretation of the data. M.L., M. Rudemo, M. Röding, and A.S. performed the statistical analysis of the data. M.A., M. Rudemo, M. Röding, N.L., J.H., and A.S. contributed to the interpretation of the results. All authors contributed to the discussion and critical revision of the manuscript.

ACKNOWLEDGMENTS

Dr. Kris Janssen (Chemistry, KU Leuven) is thanked for programming the acquisition software of the homebuilt microscope. Johan Hofkens (Molecular Imaging and Photonics, KU Leuven) is gratefully acknowledged for the usage of his imaging facilities.

Financial support from the Swedish Foundation for Strategic Research and Knut and Alice Wallenberg Foundation is highly appreciated. J.H. acknowledges the KU Leuven for funding (C14/16/053). V.L. acknowledges the UHasselt Bijzonder Onderzoeksfonds fund (BOF17DOC11) for a PhD scholarship. Guillermo Solís Fernández is grateful for a PhD scholarship from the Research Foundation Flanders.

REFERENCES

- Petersen, N. O., P. L. Höddelius, ..., K. E. Magnusson. 1993. Quantitation of membrane receptor distributions by image correlation spectroscopy: concept and application. *Biophys. J.* 65:1135–1146.
- Kolin, D. L., S. Costantino, and P. W. Wiseman. 2006. Sampling effects, noise, and photobleaching in temporal image correlation spectroscopy. *Biophys. J.* 90:628–639.
- Wiseman, P. W. 2013. Image correlation spectroscopy: Mapping correlations in space, time, and reciprocal space. In *Fluorescence Fluctuation Spectroscopy (FFS)*, Part A, volume 518 of *Methods in Enzymology*. Academic Press, pp. 245–267.
- Digman, M. A., C. M. Brown, ..., E. Gratton. 2005. Measuring fast dynamics in solutions and cells with a laser scanning microscope. *Biophys. J.* 89:1317–1327.
- Brown, C. M., R. B. Dalal, ..., E. Gratton. 2008. Raster image correlation spectroscopy (RICS) for measuring fast protein dynamics and concentrations with a commercial laser scanning confocal microscope. *J. Microsc.* 229:78–91.
- Rosow, M. J., J. M. Sasaki, ..., E. Gratton. 2010. Raster image correlation spectroscopy in live cells. *Nat. Protoc.* 5:1761–1774.
- Elson, E. L., and D. Magde. 1974. Fluorescence correlation spectroscopy. I. Conceptual basis and theory. *Biopolymers.* 13:1–27.
- Koppel, D. E. 1974. Statistical accuracy in fluorescence correlation spectroscopy. *Phys. Rev. A.* 10:1938–1945.
- Qian, H. 1990. On the statistics of fluorescence correlation spectroscopy. *Biophys. Chem.* 38:49–57.
- Wohland, T., R. Rigler, and H. Vogel. 2001. The standard deviation in fluorescence correlation spectroscopy. *Biophys. J.* 80:2987–2999.
- Saffarian, S., and E. L. Elson. 2003. Statistical analysis of fluorescence correlation spectroscopy: the standard deviation and bias. *Biophys. J.* 84:2030–2042.
- Enderlein, J., I. Gregor, ..., J. Fitter. 2005. Statistical analysis of diffusion coefficient determination by fluorescence correlation spectroscopy. *J. Fluoresc.* 15:415–422.
- Digman, M. A., and E. Gratton. 2009. Analysis of diffusion and binding in cells using the RICS approach. *Microsc. Res. Tech.* 72:323–332.
- Gielen, E., N. Smisdom, ..., M. Ameloot. 2009. Measuring diffusion of lipid-like probes in artificial and natural membranes by raster image correlation spectroscopy (RICS): use of a commercial laser-scanning microscope with analog detection. *Langmuir.* 25:5209–5218.
- Ivanchenko, S., and D. C. Lamb. 2011. Fluorescence correlation spectroscopy: principles and developments. In *Supramolecular Structure and Function 10*. J. Brnjas-Kraljević and G. Pifat-Mrzljak, eds. Springer, pp. 1–30.
- Fuller, W. 1996. *Introduction to Statistical Time Series*. John Wiley & Sons, Hoboken, NJ.
- Marriott, F. H. C., and J. A. Pope. 1954. Bias in the estimation of autocorrelations. *Biometrika.* 41:390–402.
- Scipioni, L., M. Di Bona, ..., L. Lanza. 2018. Local raster image correlation spectroscopy generates high-resolution intracellular diffusion maps. *Commun. Biol.* 1:10.
- Pawley, J. B. 2006. *Handbook of Biological Confocal Microscopy*. Springer Science, New York, pp. 59–79.
- Silverman, B. 1985. *Density Estimation for Statistics and Data Analysis*. Chapman & Hall, London, UK.
- Schrimpf, W., A. Barth, ..., D. C. Lamb. 2018. PAM: a framework for integrated analysis of imaging, single-molecule, and ensemble fluorescence data. *Biophys. J.* 114:1518–1528.
- Efron, B., and R. Tibshirani. 1993. *An Introduction to the Bootstrap*. Chapman & Hall, London, UK.
- Bates, D. M., and D. G. Watts. 1988. *Nonlinear Regression Analysis and Its Applications*. John Wiley & Sons, New York.
- Longfils, M., E. Schuster, ..., M. Rudemo. 2017. Single particle raster image analysis of diffusion. *J. Microsc.* 266:3–14.
- Hendrix, J., T. Dekens, ..., D. C. Lamb. 2016. Arbitrary-region raster image correlation spectroscopy. *Biophys. J.* 111:1785–1796.
- Kapusta, P., M. Wahl, ..., J. Enderlein. 2007. Fluorescence lifetime correlation spectroscopy. *J. Fluoresc.* 17:43–48.
- Hendrix, J., W. Schrimpf, ..., D. C. Lamb. 2013. Pulsed interleaved excitation fluctuation imaging. *Biophys. J.* 105:848–861.
- Gröner, N., J. Capoulade, ..., M. Wachsmuth. 2010. Measuring and imaging diffusion with multiple scan speed image correlation spectroscopy. *Opt. Express.* 18:21225–21237.
- Hebert, B., S. Costantino, and P. W. Wiseman. 2005. Spatiotemporal image correlation spectroscopy (STICS) theory, verification, and application to protein velocity mapping in living CHO cells. *Biophys. J.* 88:3601–3614.
- Digman, M. A., and E. Gratton. 2009. Imaging barriers to diffusion by pair correlation functions. *Biophys. J.* 97:665–673.